

DISCHARGING OF DUST PARTICLES OF DIFFERENT SIZES IN AN ARGON AFTERGLOW PLASMA

I.B. Denysenko¹, M. Mikikian², N.A. Azarenkov^{1,3}

¹V.N. Karazin Kharkiv National University, Kharkiv, Ukraine;

²GREMI, UMR7344 CNRS/Université d'Orléans, F-45067 Orléans, France;

³National Science Center "Kharkov Institute of Physics and Technology", Kharkiv, Ukraine

E-mail: idenysenko@yahoo.com

The dust charge distribution function (DCDF) in an argon plasma afterglow is obtained by solving numerically the master equation describing dust discharging as a one-step stochastic process. The calculated DCDFs are compared with Gaussian distributions, and it is found that the dust charge distribution functions can be approximated quite well by the latter ones for different external conditions. It is found how the DCDF, mean dust charge, variance and charging time depend on dust size. For late afterglow times, it is also analyzed how the emission of electrons in the collisions of excited argon atoms with dust particles affects the DCDF. It is shown that the emission effect is more essential for larger nanoparticles than for smaller ones.

PACS: 52.27.Lw, 52.25.Vy, 52.65.-y, 52.50.Dg

INTRODUCTION

Discharging of nanosized and microsized particles (dust particles) in afterglow plasmas has been analyzed in many papers [1-4]. However, most of the authors in their theoretical and numerical studies have used "continuous discharging models" [5, 6], i.e., the currents collected from the plasma, which determine the charge on a dust grain, are assumed to be continuous in time. Therefore, these models allow to calculate only the mean grain charge and do not account for its discreteness [6]. Meantime, the discreteness affects essentially the charging process and dust charge fluctuations [6, 7].

At present, there are only a few works where the discharging of dust particles in an afterglow plasma was analyzed taking into account the discreteness of the dust charge. In [8, 9], the dust charge distribution function (DCDF) of particles with radius $a_d = 190$ nm in a temporal afterglow plasma was measured and simulated using the Monte Carlo method as in [6]. In our previous work [10], the dust charge distribution function was obtained by solving numerically the master equation describing dust discharging as a one-step stochastic process. The calculated DCDFs were very close to the Gaussian solutions obtained using the approach as in [11, 12]. The calculated DCDFs were also compared with those measured in experiments [9] and were found to be in good qualitative agreement if the dust discharging model accounts for the emission of electrons in the collisions of excited argon atoms with dust particles [10]. However, in our previous work [10], we did not analyze in detail how discharging of dust particles depends on dust radius. Meantime, in experiments on dusty plasma, dust particles may have different radius and their charge depends on a_d .

In this paper, we show how the DCDF, mean dust charge, variance and dust charging time depend on dust radius. The dust charge parameters are calculated taking into account the secondary electron emission in the

collisions of excited argon atoms with dust particles. The case when the secondary emission process is neglected is also considered in our study.

1. MAIN EQUATIONS AND ASSUMPTIONS

We consider an argon afterglow plasma with radius $R = 2$ cm and height $L = 3$ cm (the plasma sizes here are the same as in [8, 9]) containing electrons with density n_e , singly charged positive ions (Ar^+) with density n_i , ground-state argon atoms (Ar_0) with density n_a , metastable argon atoms (Ar_m) with density n_m , argon atoms in the resonance 4s states ($^3\text{P}_1$ and $^1\text{P}_1$) (Ar_r) with density n_r , as well as argon atoms in 4p states (Ar_{4p}) with density n_{4p} . We assume that the plasma also contains dust particles with density $n_d = 5 \times 10^4 \text{ cm}^{-3}$, as in [9]. The ions and dust particles in the plasma are at gas temperature $T_g (= 0.026 \text{ eV})$, and the ions and electrons have Maxwellian distributions. The neutral gas pressures considered here are $P = 0.3$ and 0.9 Torr, as in [8, 9].

The plasma afterglow is analyzed using a 0D model. The model includes the balance equations for electrons, ions and argon atoms in different excited states, which can be presented in the following form:

$$\frac{\partial n^{(X)}}{\partial t} = \sum_i R_{G,i}^{(X)} - \sum_i R_{L,i}^{(X)}, \quad (1)$$

where t is the afterglow time, $n^{(X)}$ is n_e , n_i , n_m , n_r or n_{4p} . $R_{G,i}^{(X)}$ and $R_{L,i}^{(X)}$ are, respectively, the rates for reactions of the various generation and loss processes of the species with density $n^{(X)}$. The reactions taken into account in the model to calculate the electron, ion, metastable, 4s resonant and 4p atoms densities, as well as their rate coefficients are described in detail in [10]. The model also accounts for the transition from ambipolar to free diffusion and for multistep ionization and excitation and

deexcitation of argon atoms in the plasma afterglow [10]. Considering the electron diffusion in the afterglow plasma, it is assumed that the electron diffusion coefficient is connected with the ambipolar diffusion coefficient and Debye electron length as in [9, 10] for the fast transition case.

The electron temperature T_e as a function of time in the plasma afterglow is obtained from the power balance equation:

$$\frac{\partial}{\partial t} \left(\frac{3}{2} en_e T_e \right) = \frac{(P_{\text{abs}} - P_{\text{loss}})}{V}, \quad (2)$$

where e is the elementary charge, P_{abs} is the power absorbed in the plasma volume V in the power on phase ($t = 0$) and $P_{\text{loss}} \approx P_w + P_{\text{coll}}$. P_w and P_{coll} are the power loss on the walls and the power loss in electron neutral collisions, respectively [10]. Here, the power P_{abs} is chosen to have $n_e(t = 0) = 5.0 \times 10^9 \text{ cm}^{-3}$, as in [9]. In the plasma afterglow, $P_{\text{abs}} = 0$.

It is assumed that the dust particles in the plasma afterglow are of the same radius a_d , but may have different charges due to stochastic charge fluctuations connected with charge discreteness. The dust charges are characterized by the DCDF F_k , which can be found from the following master equation [7, 11]:

$$\begin{aligned} \frac{d}{dt} F_k &= v_{ed}^{k+1} F_{k+1} - v_{ed}^k F_k - (v_{id}^k + v_m) F_k + \\ &(v_{id}^{k-1} + v_m) F_{k-1}, \end{aligned} \quad (3)$$

where v_{ed}^k and v_{id}^k are the frequencies with which a particle with charge $Z_d^k = ke$ collects electrons and ions [10], respectively, k is an integer. v_m is the frequency describing electron emission from the dust surface at collisions of dust particles with argon atoms in excited states. The DCDF is normalized by $\sum_k F_k = 1$.

The mean dust charge Z_d is calculated using the following expression

$$\frac{\partial Z_d}{\partial t} = v_{id} + \gamma_m K_m^d (n_m + n_r + n_{4p}) - v_{ed}, \quad (4)$$

where v_{id} and v_{ed} are coinciding with the corresponding expressions for v_{id}^k and v_{ed}^k if one replaces in these expressions Z_d^k by Z_d . K_m^d is the rate for collisions of excited argon atoms with dust particles [10], and γ_m is the corresponding yield describing the induced secondary electron emission.

The DCDF calculated from equation (3) is compared with the Gaussian distribution [11, 12]:

$$F_{Gk} = \frac{1}{(2\pi\sigma_z^2)^{1/2}} \exp \left[-\frac{(-Z_d^k + Z_d)^2}{2\sigma_z^2} \right], \quad (5)$$

where Z_d is determined by equation (4), while the variance σ_z^2 is obtained from the following equation [11, 12]:

$$\frac{d\sigma_z^2}{dt} \approx -\alpha'_1 \sigma_z^2 + \alpha_2, \quad (6)$$

where $\alpha'_1 = 2(v'_{ed} - v'_{id})$ with primes indicating derivatives with respect to Z_d , $\alpha_2 = v_{ed} + v_{id} + v_m$.

The equations (1) – (4) and (6) are solved numerically by using the DVODE package [13]. The initial values of plasma parameters, except $n_e(0)$ and $n_i(0)$, are obtained setting $\partial/\partial t = 0$ in the model equations. It is assumed that at $t = 0$, $n_e = n_i = 5 \times 10^9 \text{ cm}^{-3}$, as in [9].

2. NUMERICAL RESULTS

Using Eqs. (1) – (4), (6), we calculated the dust charge distribution function, mean dust charge, variance and charging time $\tau_{ch} = 1/[v'_{ed} - v'_{id}]$ as functions of time. The calculations were carried out for the conditions close to those in [9]. The results were obtained taking into account secondary electron emission in the collisions of excited argon atoms (Ar_m , Ar_r and Ar_{4p}) with dust particles ($\gamma_m \neq 0$), as well as neglecting by this process ($\gamma_m = 0$). Note that we used in our simulations the values of γ_m leading to a good agreement with experimental data [9], while the exact values of γ_m are not known for the conditions considered here. The simulations were carried out to analyze how the parameters of dust charge depend on dust size.

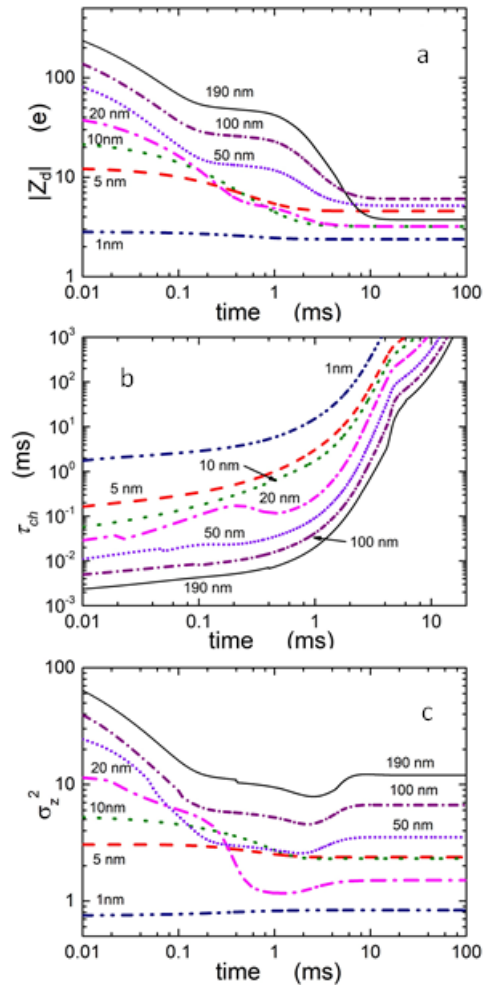


Fig. 1. $|Z_d|$ (a), τ_{ch} (b) and σ_z^2 (c) as functions of time for $P = 0.3 \text{ Torr}$, $\gamma_m = 0.035$ and $a_d = 1, 5, 10, 20, 50, 100$, and 190 nm

Fig. 1,a shows the absolute value of mean dust charge as a function of time for different dust radii. The initial $|Z_d|$ increases if a_d becomes larger (see Fig. 1,a) because of larger surface collecting electrons from the plasma volume. $|Z_d|$ decreases faster with time in the beginning of afterglow, if dust size increases (see Fig. 1,a). The faster decrease of $|Z_d|$ is mainly because of larger ion flux to the dust particle surface ($v_{id} \sim a_d^2$). Due to larger ion and electron fluxes to a dust particle, the charging time decreases when a_d becomes larger (see Fig. 1,b). Therefore, at late afterglow times, the absolute value of mean dust charge may become smaller with increasing a_d (see Fig. 1,a). In particular, $|Z_d|$ for $a_d = 5$ nm is larger than the absolute values of mean dust charge for $a_d = 10$ and 20 nm. This is mainly due to smaller v_{id} in the $a_d = 5$ nm case compared with the frequencies in the $a_d = 10$ and 20 nm cases. Moreover, the secondary emission in metastable-dust collisions affects more essentially the charge of larger dust particles. At late afterglow times ($t = 100$ ms), $|Z_d|$ is 2.37 (2.37), 4.61(4.56), 3.36(3.2), 3.59(3.2), 6.8(5.17), 10.7(6.04), 16.08(3.74) for $a_d = 1, 5, 10, 20, 50, 100, 190$ nm at $\gamma_m = 0$ ($\gamma_m = 0.035$), respectively. Thus, at $t = 100$ ms and $\gamma_m = 0.035$, the absolute value of mean dust charge for $a_d = 190$ nm is smaller than $|Z_d|$ for $a_d = 5, 50$ and 100 nm because of the secondary emission. This is not the case for $\gamma_m = 0$. The effect of secondary emission on dust charge enhances with increasing dust radius because the rate for metastable-dust collisions increases with increasing a_d ($K_m^d \sim a_d^2$).

Note that at late afterglow times, the mean charges of dust particles with different a_d may be nearly the same (see $|Z_d(t)|$ in (see Fig. 1,a) for $a_d = 10$ and 20 nm), while the variances are very different (see Fig. 1,c). Similarly, the variances for different a_d may be nearly the same (see σ_z^2 in (see Fig. 1,c) for $a_d = 5$ and 10 nm), while the mean charges differ essentially (see Fig. 1,a). In our opinion, this is due to changes in the dust charging time and the variance at a variation of a_d . For large dust particles ($a_d \geq 20$ nm) and $t \geq 0.3$ ms, the variance increases with growth of a_d (see Fig. 1,c). This conclusion can be also obtained using the orbit motion limited (OML) approximation for the steady-state case at $\gamma_m = 0$

$$\sigma_z^2 \approx \frac{(1 + v_{ed}/v_{id})a_d T_e}{2e(\tau/(1+\tau|z|) + v_{ed}/v_{id})} \propto a_d, \quad \text{where } \tau = T_e/T_i, \quad T_e$$

and T_i are the electron and ion temperatures, respectively, and $z = eZ_d/a_d T_e$). The variance depends also on γ_m , and at late afterglow times for large dust particles, σ_z^2 in the case of $\gamma_m = 0.035$ is larger than that in the case of $\gamma_m = 0$. At $t = 100$ ms, the variance is 0.83(0.83), 2.34(2.37), 2.21(2.3), 1.28(1.5), 2.67(3.52), 4.51(6.65) and 7.36(11.99) for $a_d = 1, 5, 10, 20, 50, 100, 190$ nm at $\gamma_m = 0$ ($\gamma_m = 0.035$), respectively. The dependence of the variance in the afterglow plasma is the same as that in the steady-state case [7, 10]

$$\left(\sigma_z^2 \approx \frac{v_{ed} + v_{id} + \gamma_m K_m^d (n_m + n_r + n_{4p})}{2(v_{ed}' - v_{id}')} \right),$$

i. e., it is increasing with an increase of γ_m .

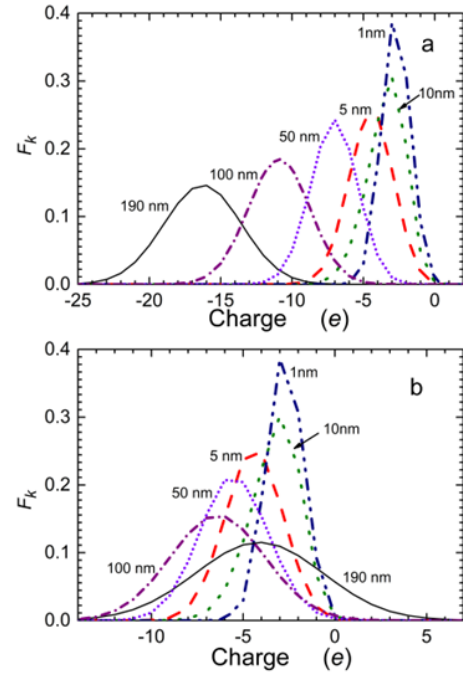


Fig. 2. The DCDFs calculated for different dust radii at $\gamma_m = 0$ (a) and when $\gamma_m = 0.035$ (b). The other conditions are the same as in Fig. 1

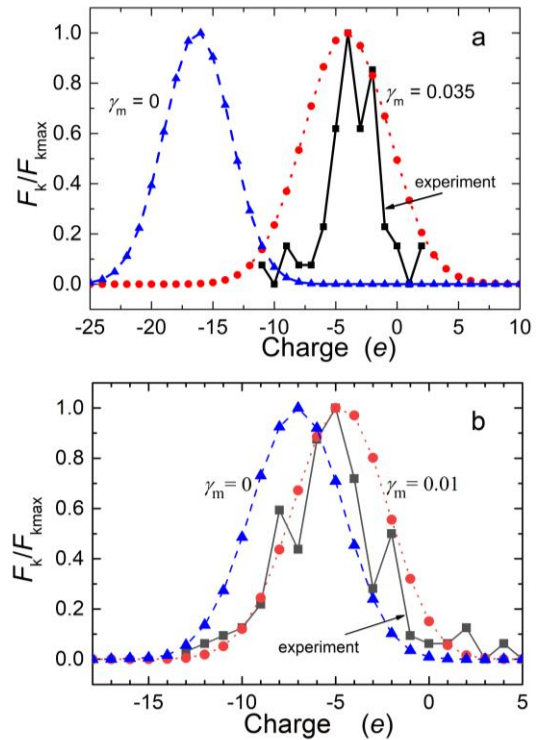


Fig. 3. The normalized DCDFs for $P = 0.3$ Torr (a) and $P = 0.9$ Torr (b). The distributions are calculated at $\gamma_m = 0$ (dashed curves) and $\gamma_m \neq 0$ (dotted curves). The solid curves correspond to the DCDFs obtained in experiments [9]. Here, $F_{kmax} = F_k(Z_{dmax}^k)$, $a_d = 190$ nm and the other conditions are the same as in Fig. 1. Z_{dmax}^k is the charge corresponding to the maximum of F_k

Using the master equation (3), we also calculated the dust charge distribution at late afterglow times for $\gamma_m = 0$ (Fig. 2,a) and $\gamma_m = 0.035$ (see Fig. 2,b).

Fig. 2,a shows that most dust particles in the $\gamma_m = 0$ case are negatively charged, independently on their size. Meantime, rather large amount of dust particles with $a_d = 190$ nm are positively charged in the $\gamma_m = 0.035$ case, while the particles of smaller size are mainly negatively charged. This is because the variance for large dust particles is larger and $|Z_d|$ is smaller in the $\gamma_m = 0.035$ case compared with the corresponding values obtained at $\gamma_m = 0$ (see Fig. 1 and [14]). For small $a_d (\leq 10$ nm), the dust charge distribution function in the $\gamma_m = 0.035$ case is nearly the same as that obtained for $\gamma_m = 0$, because σ_z^2 and $|Z_d|$ are also nearly the same in the both cases.

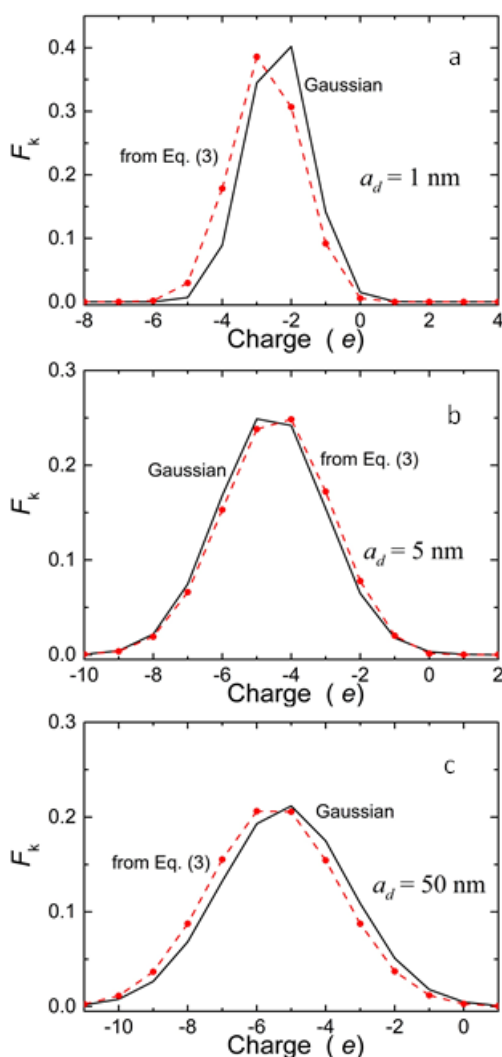


Fig. 4. The DCDFs obtained from Eq. (3) (dashed curves) and from Eqs. (5) and (6) (solid curves) for $a_d = 1$ nm (a), 5 nm (b), and 50 nm (c). Here $P = 0.3$ Torr, and the other conditions are the same as in Fig. 1

We also compared the dust charge distribution functions, which were obtained for late afterglow times and $a_d = 190$ nm from Eq. (3), with those measured in experiments [8, 9] at $P = 0.3$ Torr (Fig. 3,a) and $P = 0.9$ Torr (see Fig. 3,b). It was found that the calcu-

lated DCDFs agree well with the measured ones [9], if our model accounts for the secondary emission with $\gamma_m = 0.035$ for $P = 0.3$ Torr (see Fig. 3,a) and with $\gamma_m = 0.01$ for $P = 0.9$ Torr (see Fig. 3,b).

For late afterglow times ($t = 100$ ms), we also compared the DCDFs calculated from the master equation (3) with the Gaussian distributions obtained using Eqs. (4) - (6). It is found that F_{Gk} approximates rather well the DCDF obtained from the master equation (3) for different dust radii (Fig. 4). Slight differences are due to the fact that the Gaussian distributions were obtained assuming that the variance is essentially smaller than Z_d^2 (see [11, 12]), which is not the case for the conditions here (see Fig. 1).

CONCLUSIONS

Discharging of dust particles of different sizes in an argon plasma afterglow has been investigated. It has been analyzed how the DCDF, mean dust charge, variance and charging time depend on dust radius. It has been shown that the absolute value of mean dust charge decreases faster with time in the beginning of afterglow if the dust size is larger because of larger ion flux to the dust particle surface. Due to larger ion and electron fluxes to a dust particle, the dust charging time decreases when a_d becomes larger (see Fig. 1,b). As a result, at late afterglow times, the absolute value of mean dust charge may become smaller with increasing a_d (see Fig. 1,a). Moreover, it has been also found that the secondary emission in metastable-dust collisions affects more essentially the charge of larger dust particles. This is because of large rate for collisions of excited argon atoms with dust particles. It has been obtained that for $t \geq 0.3$ ms and large dust particles ($a_d \geq 20$ nm), the variance increases with growth of a_d (see Fig. 1,c). For late afterglow times, the variance is larger in the presence of the secondary emission than in the case when $\gamma_m = 0$. The results concerning the variance in the afterglow plasma are in agreement with the conclusions obtained using analytical expressions for σ_z^2 in the steady-state case.

The calculated dust charge distribution functions have been compared with the measured ones [9] and have been found to be in good qualitative agreement if the dust discharging model accounts for the emission of electrons in the collisions of excited argon atoms with dust particles (see Fig. 3).

The DCDFs calculated from the master equation (3) have been compared with the Gaussian distributions obtained using the approach in [11, 12]. It has been found that the Gaussian distributions approximate rather well the calculated DCDFs for different dust radii (see Fig. 4).

The results presented here are relevant to many applications involving plasmas [15-17], especially gas discharges used for the synthesis of various nanomaterials.

ACKNOWLEDGEMENTS

The work was partially supported by Le Studium (Loire Valley Institute for Advanced Studies, 45000 Orléans, France).

REFERENCES

1. B. van Minderhout, J.C.A. van Huijstee, R.M.H. Rempelberg, A. Post, A.T.A. Peijnenburg, P. Blom, J. Beckers // *Nat. Commun.* 2021, v. 12, p. 4692.
2. L. Couëdel, M. Mikikian, L. Boufendi, A. A. Samarian // *Phys. Rev. E.* 2006, v. 74, p. 026403.
3. I.B. Denysenko, I. Stefanović, B. Sikimić, J. Winter, N.A. Azarenkov // *Phys. Rev. E.* 2013, v. 88, p. 023104.
4. N. Chaubey, J. Goree // *Front. Phys.* 2022, v. 10, p. 879092.
5. J. Goree // *Plasma Sources Sci. Technol.* 1994, v. 3, p. 400.
6. C. Cui, J. Goree // *IEEE Trans. Plasma Sci.* 1994, v. 22, p. 151.
7. T. Matsoukas, M. Russell, M. Smith // *J. Vac. Sci. Technol. A.* 1996, v. 14, p. 624.
8. L. Couëdel, A.A. Samarian, M. Mikikian, L. Boufendi // *EPL.* 2008, v. 84, p. 35002.
9. L. Couëdel, A.A. Samarian, M. Mikikian, L. Boufendi // *Phys. Plasmas.* 2008, v. 15, p. 063705.
10. I.B. Denysenko, M. Mikikian, N.A. Azarenkov // *Phys. Plasmas.* 2022, v. 29, p. 093702.
11. B. Shotorban // *Phys. Rev. E.* 2011, v. 83, p. 066403.
12. B. Shotorban // *Phys. Plasmas.* 2014, v. 21, p. 033702.
13. S.P. Corwin, S. Thompson, S.M. White // *J. Numer. Anal. Indust. Appl. Math.* 2008, v. 3, p. 139.
14. I. B. Denysenko, M. Mikikian, N.A. Azarenkov // *J. Phys. D.* 2022, v. 55, p. 095201.
15. M.A. Lieberman, A.J. Lichtenberg. *Principle of Plasma Discharges and Material Processing.* New York: "Wiley", 2005.
16. I. Denysenko, M.Y. Yu, L. Stenflo, S. Xu // *Phys. Rev. E.* 2005, v. 72, p. 016405.
17. N.A. Azarenkov, I.B. Denysenko, A.V. Gapon, T.W. Johnston // *Phys. Plasmas.* 2001, v. 8, p. 1467.

Article received 03.10.2022

РОЗРЯДЖАННЯ ПОРОШИНОК РІЗНОГО РОЗМІРУ В АРГОНОВІЙ ПЛАЗМІ ПІСЛЯСВІТІННЯ

І.Б. Денисенко, М. Мікікіан, М.О. Азаренков

Здобуто функцію розподілу порошинок за зарядом (ФРПЗ) у післясвітінні аргонової плазми шляхом числового розв'язання основного кінетичного рівняння, що описує розрядження порошинок як однокроковий стохастичний процес. Розраховані ФРПЗ порівняно з розподілами Гаусса, і виявлено, що останні можуть доволі добре описувати функції розподілу порошинок за зарядом за різних зовнішніх умов. З'ясовано, як ФРПЗ, середній заряд порошинок, дисперсія функції Гаусса, що апроксимує ФРПЗ, та час заряджання порошинок залежать від розміру порошинок. Для пізніх часів післясвітіння також аналізується, як емісія електронів у зіткненнях збуджених атомів аргону з порошинками впливає на ФРПЗ. Показано, що вплив цієї емісії на більші порошинки є більш суттєвим, ніж на малі.